Iranian Journal of Physics Research, Vol. 21, No. 3, 2021

Investigation of structural and Magnetic properties of (Nb) Substituted YBCO-system

R Hajilou and H sedghi
Department of physics, Superconductivity Research Center, Urmia University, Urmia, Iran

E-mail: rahil.hajilou@yahoo.com

(Received 16 August 2019 ; in final form 02 January 2021)

Abstract
In this study, we report the synthesis and characterization of $YBa_2Cu_3O_{7-\delta}$ (YBCO) high temperature superconductor prepared by solid state method and doped with Nb in different weight percentages, 0, 0.01, 0.02 and 0.05 wt%. The x-ray diffraction (XRD) analysis confirms the formation of orthorhombic phase of superconductivity for all the prepared samples. We evaluated the effects of Nb doping on the normal state resistivity (ρ), superconducting transition temperature (Tc), scanning electron microscope (SEM. The critical current densities, J_C as a function of temperature have been calculated using the critical state model from the hysteresis loops up to 1T at temperature range of 10K to 60K. Magnetic flux pinning, F_P of samples was calculated by using Lorentz force. XRD analysis show a shorter c axis parameter and higher orthoromthcity than the pure Y-123 and other Nb doped samples. It was also found from critical current density and magnetic flux pinning force measurement the 0.01 wt% Nb substation for Y on YBCO superconductors improve the critical current density and flux pinning force.

Keywords: H-T Superconductors, X-Ray diffraction, SEM, Hysteresis loops, Critical Current Density and Flux pinning

1. Introduction

Following the discovery of high-temperature superconductivity (HTSc) by Bednorz and Muller [1] in metal oxide cuprates, lot of similar materials have been explored with high values of superconducting transition temperature (T_c). The discovery of superconductivity in Y-Ba-Cu-O system with transition temperature above 90 K was one of the great achievements in the field of high temperature superconductivity [2]. Although, these materials possess high transition temperature, the practical applications of these materials are yet scant due to relatively inferior values of some superconducting parameters such as critical current density (J_C) and upper critical field [3]. The analysis of impurity effects in high temperature (HTSC) gained additional interest upon confirmation that this subject could provide a crucial test for d-wave symmetry of the order parameter in high T_c copper oxides [4, 5]. It is well known that the oxygen content affects the crystal structure electronic transport and superconducting properties in YBCO. It is also realized that the superconducting transition temperature, T_c, sensitively depends on both the hole concentration in the CuO_2 planes and the relative electric charge of the oxygen within the planes [6, 7]. The level of this charge can be controlled either by manipulating the oxygen stoichiometry in the Cu–O chains, by application of pressure or by ionic substitution [8, 9]. Therefore, lot of efforts had been put towards discovery of superconducting materials with higher critical parameters. The major limiting factors in case of practical applications of most HTSC systems are inter-grain weak links and poor flux pinning capability. From this point of view, the investigation on the Ca doped YBCO ($YBa_2Cu_3O_{7-\delta}$) system is of great interest. Calcium ion (Ca^{2+}) preferentially substitutes for Yttrium ion (Y^{3+}) because of it's ionic radius being closer to that of Yttrium [10-11].

In this research, our aims are:

1) To answer this question that substitution with Nb in YBCO systems increases or decreases the critical temperature.

2) To explore the magnetic behavior of the modified $Y_{1-x}Nb_xBa_2Cu_3O_{7-\partial}$ systems. In other words, this substitution improves or depresses the superconductivity of $Y_{1-x}Nb_xBa_2Cu_3O_{7-\partial}$ systems.

2. Experimental

All samples were synthesized through the conventional solid state reaction route. High purity powders of Y_2O_3, Nb_2O_5, $BaCO_3$, CuO (99.99%) with the exact stoichiometric ratio were mixed. The appropriate amounts of the powders were ground thoroughly by hand using an agate mortar and pestle for 1hr. The thoroughly mixed powders were then pelletized by pressing into a 30mm diameter steel die (carver 4387. 4SD0B00) under 40 MPa pressure. The pellets were then quickly loaded on to an alumina tile and placed into a furnace where they were subjected to a heat treatment. The samples in the furnace were heated to 720 ^{0}C at the rate of 120^{0}C/h and heated at 720^{0}C for 12 hours followed by heating to 930^{0}C at the rate of 120^{0}C/h and were annealed at 930^{0}C for 12 hours. Finally the samples were furnace cooled to room temperature. After this first sintering process, all the samples had a dark color. In this sintering process none of the products were good quality samples. They could be easily separated into several layers. Therefore, in order to make quality and fully oxygenated samples, the sintering process was repeated. In the second cycle of the heating process, the samples were re-ground and pressed into pellets with a 30 mm diameter and approximate thickness of 3 mm under 60 MPa pressure. Pellets were then placed into a furnace and heated 930^{0}C at the rate of 90^{0}C/h. They were left to react at this temperature for 24 hours. Finally, the temperature was decreased 720^{0}C at a rate of 20^{0}C/h and then furnace-cooled to room temperature in flowing oxygen with a cooling rate of 10^{0}C/h. Low cooling rate in flowing oxygen was used in order to improve oxygen uptake in the samples. Unlike the first processing cycle, the products of the second cycle were uniform and almost with any cracks X-ray diffraction measurements were made in the range of 2θ =5˚- 60˚ with CuKα radiation source (λ=1.5406A˚). Using x-pert pro Philips analytical diffractometer, XRD results were used in the powder diffraction programmer in order to determine a, b, c lattice parameters of the samples. The size and surface morphology of grains were analyzed by scanning electron microscopy (SEM). The resistivity measurements were carried out by standard four-probe method using low frequency/low AC current over the temperature range 20–100 K. Electrical contacts were made using conducting silver paint. The critical current density, J_c was calculated using the Bean model for pure and Nb substituted x=0.01 samples at 10-60K up to 60KG applied magnetic field. The pinning force, F_p depending on applied magnetic field and temperature was calculated from isothermal M-H measurement.

3. Result and Discussions

3.1 XRD results

In order to investigate the structure of the samples and ensure the formation of the desired phase, the x-ray diffraction spectrum was investigated. It was observed from the comparison of the spectrum of contaminated samples with Nb by the pure sample (x=0.0) that in some of the contaminated samples were removed a number of peaks related to the optimal phase 123, and instead of that, the unwanted phase peaks of 211, along with the secondary peaks of the lead impurity, appeared in the samples spectrum of diffraction patterns. The peaks of the undoped sample (YBCO) and Nb doped sample $Y_{1-x}Ba_2Cu_3Nb_xO_{7-\sigma}$ were well matched to the orthorhombic Y123 structure. As can be seen there is a slight difference in the patterns for the sample with x = 0.00 compared to the Nb doped samples. The peaks were observed at about 29.8 degrees and about 53.1 degrees and the intensity of these peaks increased gradually with the increasing of Nb content. These peaks were identified as due to niobium perovskite. With increasing Nb content samples gave a diffused phase indicating a niobium perovskite phase [12]. An insignificant peak belonging to the non-superconducting phase $BaCuO_2$ appears at 2θ ~30˚ [13]. The double peaks at 2θ ~46.5° with increasing x show a clear evolution towards a triplet peak structure, which has been identified with the appearance of an orthoromthcity II phase. As shown in the next section, the increase of x leads to an increase in oxygen loss for all the four of samples (see Table I). For the (006) peak 2θ ~46.5°, by increasing x value, the intensity has been deceased. Another interesting feature occurs at 2θ ~58° see Fig.1 (a) and (b), where the relative intensity of the double peak structure shows a change with increasing x. For Nb based series, the intensity of (123) peak in 2θ ~58° for x=0.00, 0.01, 0.02, and 0.05 samples has been increase respectively. The Rietveld refinement of the XRD data, shows that all the samples show orthorhombic symmetry. The oxygen content of the samples were determined by the Wolf's method, 7-σ =76.4 -5.95 C (A°) using the c axis lattice parameter of the samples [14]. It is well known that both the a and b lattice parameters in YBCO system have a nonlinear relationship in the orthorhombic phase, while the c-axis lattice parameter and unit-cell volume, show a generally linear behavior as a function of oxygen content. The higher the oxygen content of sample is the lower the c-axis lattice parameter [15]. The calculated unit cell parameters of the pure and the Nb substituted samples, orthorhombic strains, Δ= (b-a) / (b+a) and transition temperature of the samples are listed in table 1. It may be seen from this table that although the unit cell parameters of the alloyed samples are very close to the Y_{123} sample and there is a very little changes in a and b lattice parameters of the samples, a small increase in c-axis length shows a slight decrease in oxygen content in the samples. The small decrease in c axis parameter is probably relate to difference in (007) refection in XRD patterns of this sample. The difference on the unit cell parameters can be due to occupation of the Nb ions to interstitial sites [16]. The crystallite size of the samples was calculated by using of Debby-Scherrer equation [17].

$$L_{h\,kl} = (0.9\,\lambda) / (\beta_c \cos(\theta)) \quad (1)$$

Where β_c is the peak width at half maximum of X-ray peaks in radians, λ is the wavelength of the incident radiation ($\lambda_{cuk\alpha}$=1.54056 A°), and θ is the angle of the peak position. These values for all the prepared samples are shown in Table1. The results clearly show that there is a decreasing trend in the values of crystallite size with addition of Nb with x>0.01 in the fabricated compounds. We also have calculated the hole-carrier concentration

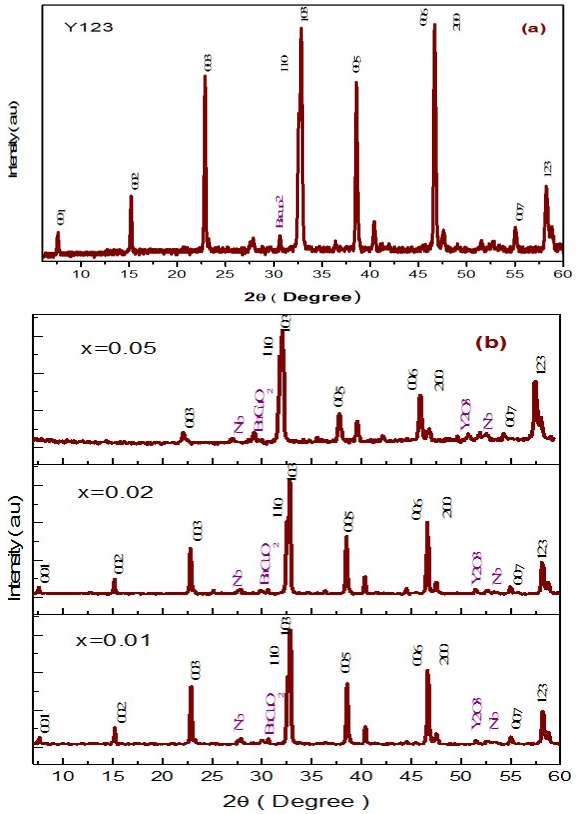

Fig 1. (a) and (b) XRD patterns of Y1-xNbxBa2Cu3O7-∂ samples with x =0.0, 0.01, 0.02 and 0.05.

Table 1. Characteristic temperatures, lattice parameters, grain size and orthorombicity parameters for all the $Y_{1-x}Nb_xBa_2Cu_3O_{7-\partial}$ samples.

Nb	Tc.onset (K)	Tc.offset (K)	ΔT_c (K)	O-content	grain size (nm)	a (A°)	b (A°)	c (A°)	p	Δ= (b-a)/(b+a)×100
x=0.00	89	82	9	6.90	40.1	3.8220	3.88	11.68	0.1908	0. 7792
x=0.01	87.5	81.2	6.3	6.8832	55.1	3.8220	3.887	11.683	0.1895	0. 843
x=0.02	82.59	76.5	6.09	6.78	34.1	3.826	3.881	11.701	0.1898	0. 717
x=0.05	80.98	74.9	6.05	6.66	32	3.8498	3.892	11.722	0.1901	0. 5502

per Cu ion, P for our studied samples using a parabolic formula which is generic to the whole class of high T_c superconductors as follows [18-19]: $[T_C(x) / T_C(0)]=1-82.6 (P-0.16)^2$. Where T_C (0) and $T_C(x)$ are the critical temperatures for pure and doped samples, respectively, P is the hole-carrier concentration per Cu ion. The calculated values of P for the studied sample are listed in table1. These values for all the prepared samples are tabulated at Table1. It is clearly observed a decreasing trend in the values of crystallite size with addition of Nb in YBCO compound.

3. 2. Analyze SEM

These SEM micrographs provide us with data about the formation of the surface morphology of the samples. Surface morphology micrographs taken by SEM for all samples are shown in Fig.2. It is well known that in high Tc superconductors, the formation and size of the superconducting grains and deliberately introduced impurities play an important role in electrical conductivity and magnetic properties of the system both in the normal and superconducting states [20]. The sample (x=0.05) has a non-uniform surface in which the grains are randomly oriented and bonded between grains is weak. The number of fine grains in the sample and the reduction in grain size indicate increased strength and hardness of the contaminated samples. It was found that the two samples (x=0.01, 0.02) have a uniform

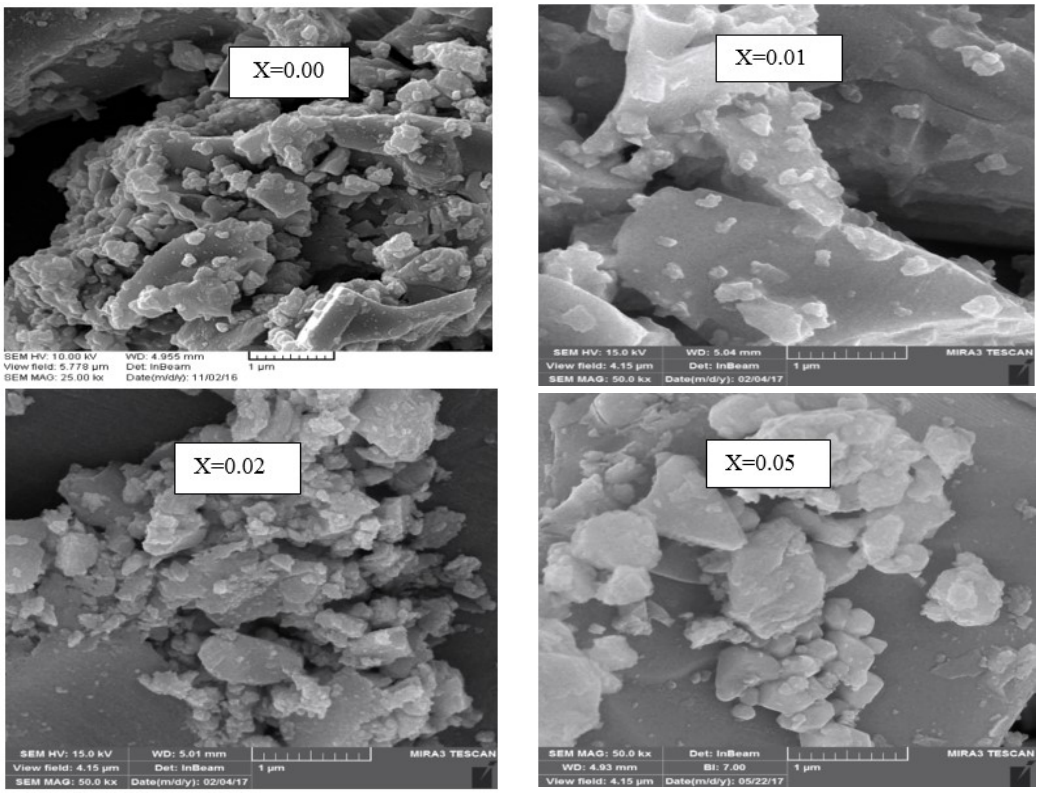

Fig 2.

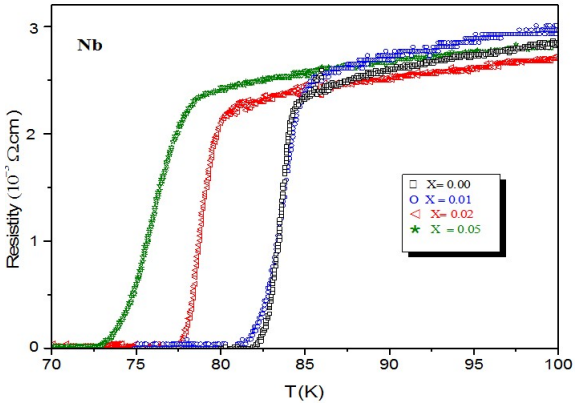

Fig 3. R-T curves of the$Y_{1-x}Nb_xBa_2Cu_3O_{7-\partial}$ with x=0, 0.01, 0.02 and 0.05.

appearance with less porosity and larger grain size, crystallization and better inter-granular bonding. As it can be seen from the figures, with increasing the amount of Nb substituted, grain size and inter-granular interactions have increased, and the porosity of the samples.

3. 3. Electrical resistance

The resistivity ρ of the $Y_{1-x}Nb_xBa_2Cu_3O_{7-\partial}$ Samples (x=0, 0.01, 0.02 and 0.05) have been measured over the temperature range 20-100K. Good linear behavior and the metallic behavior for all the samples were observed with $T \leq 89$ K. The increase in the normal state resistance as for Nb in the comparison with $0.00 \leq x \leq 0.05$ could be attributed to the corresponding absence. It is clear from Fig.2 that such with increase doping the resistivity tails and dose measurably influence the main, steep part of the resistive transition and lower temperature transition for an individual composite with an increase in the transition width ΔT. Table.1 also shows calculated values of critical transition temperatures (T, onset, Tc, offset), transition width ΔT of the pure and substituted samples.

3. 4. Magnetic properties

When the applied magnetic field is increased from zero to a specific value and then returned through zero, the hysteresis behavior can be observed. The reason of this irreversible manner of magnetization can be due to flux trapping in superconducting samples, which a crucial importance on critical current density. Fig 5(a) and 5(b) show the M-H curves of the samples at six different

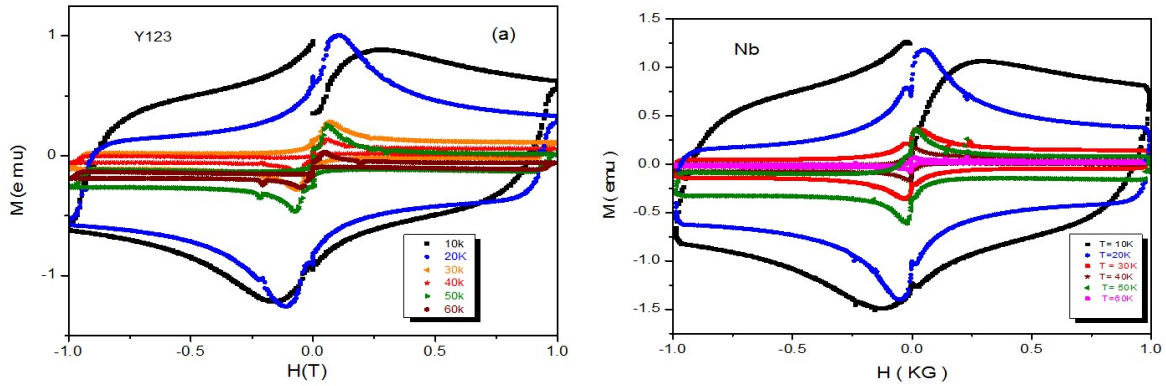

Fig 4. Displays the isothermal magnetization versus filed curves (M-H loop) at 10K, 20K, 30K, 40K, 50K and 60K for the (a) the pure Y123 and (b) the Nb x=0.01 samples

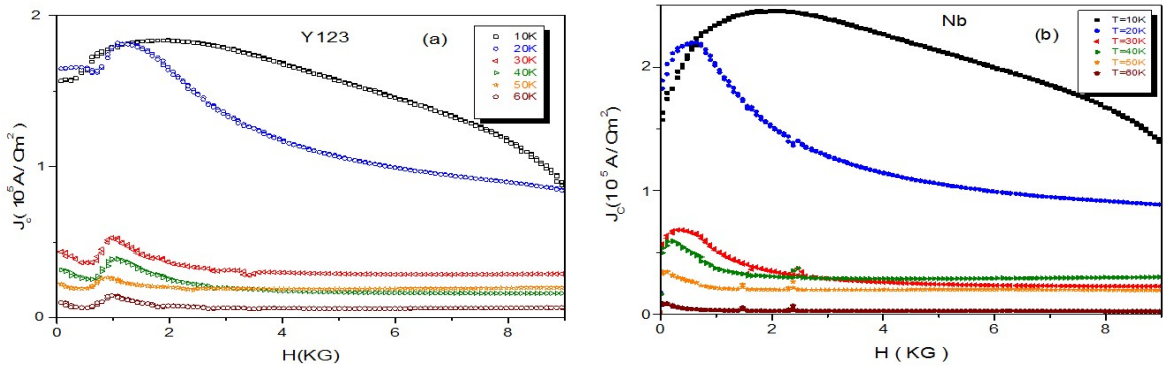

Fig 5. The plot of J_c as a function of magnetic field for (a) the pure Y123 and (b) the Nb doped x= 0.01 samples.

temperatures 10K, 20K, 30K, 40K, 50K and 60K between applied fields of 10KG. It is well established that as the critical current density decreases with increasing temperature, the hysteresis loops become narrower. This behavior is clearly seen in Fig.5 (a) and 5(b). The bigger the pinning strength, the bigger the critical current, hence the wider the hysteresis loops. It is well known that the width and behavior of this hysteresis loop is characteristics of the bulk critical current density in HTSC's and its dependence on the magnetic flux density [21]. The wider the hysteresis loop is, the higher bulk critical current density will be. By using Bean's critical state model, critical current density (J_c) of samples were calculated from the hysteresis loops [22]. In Bean's critical state model, critical current density proportional to the width of hysteresis loop $\Delta M = |M_+ - M_-|$ and calculates with this formula:

$$J_C = 20\frac{\Delta M}{a(1-a/3b)} \qquad (2)$$

In this formula, Jc is the critical current density in amperes per square centimeter of a sample and M_+ and M_- magnetizations are obtained from the intersections of M-H loops. ΔM is measured in electromagnetic units per cubic centimeter. Where a and b (a>b) are the sample dimensions perpendicular to the applied field. The maximum J_c value was determined to be 2.4×10^5 A/cm^2 at 10K for the applied magnetic field of 10KG for the Nb doped x=0.01 sample, whereas the maximum J_c value is 1.8×10^5 A/cm^2 at 10K for the same applied magnetic field for the pure Y123 sample. In the case of measuring temperature at 10K for the 10KG magnetic field, the J_c is about 1.3 times that of the pure sample. The J_C values decrease with increasing the applied magnetic field and increasing the constant measuring temperature as is clear from Fig.5. The Lorentz force, F_L, [23] is

$$F_L = J_c \times B \qquad (3)$$

Where J_C is the current density and B the flux density in the sample. We have calculated the magnetic field dependence of pinning force F_p for both the pristine Y123 and the Nb doped x=0.01 Samples. We have calculated the magnetic field dependence of pinning force F_p for both the pristine Y123 and the Nb doped x=0.01 Samples. The variation of F_p as a function of the applied magnetic field at 10K, 20K, 30K, 40K, 50K and 60K is shown in Fig. 6(a) and (b). This Fig. clearly shows that the pinning force increases with applied magnetic field at all measuring temperature for both the samples. Comparison of the figures 6(a) for pure Y123 and (b) for Nb substituted sample show that the values of pinning force in partial doping of the Y123 with Nb: x=0.01 is considerably higher than that of the pristine sample over the entire range of the applied magnetic field at each desired measuring temperature. The maximum F_P value was determined to be 1.34×10^6 N/cm^3 at 10K for the applied magnetic field of 10KG for the Nb doped x=0.01 sample, whereas the maximum F_P value is 0.96×10^6 N/cm^3 at 10K for the same applied magnetic field for the pure Y123 sample. In the case of measuring temperature at 10K for the 10KG magnetic field, the pinning force is about 1.39 times that of the

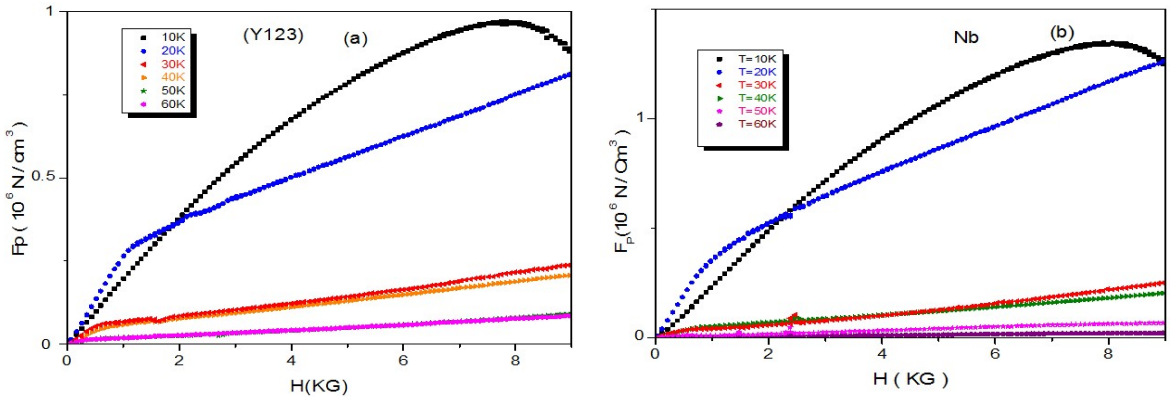

Fig 6. F_P-H dependence's at 10K, 20K, 30K, 40K, 50K and 60K (a) for the pure Y123 and (b) Nb doped x=0. 01 samples.

pure sample. These values of F_p are significantly higher than the values found in YBCO: Se composites fabricated at different temperatures under oxygen atmosphere [24]. It is well known that when Lorentz force acting the fluxoids exceeds pinning energy, F_p of the flux line lattice, the fluxoids begin to move across the sample and the material goes to resistive state. We note that Nb doped x=0.01 sample shows transition temperature higher and critical current density than that of the pure Y123 sample. The Nb atoms in Y123 system apart from improving the grain-boundary, may be acts as artificial pinning centers which itself results in the enhancement of J_c and dominance of the pinning force over the Lorentz force even at high magnetic fields. Some other research groups [25-27] found the similar behavior in Y123 system and reported that partial doping of the Y^{+3} in the Y123 with Cu^{+2} increases grain boundary J_c, which itself causes increase in pinning force.

4. Conclusions

In summary, the nominal composition of the effect of Nb doped on the superconductivity properties and the structural parameters at $Y_{1-x}Nb_xBa_2Cu_3O_{7-\sigma}$ system with doping rang $0.00 \leq x \leq 0.05$ has been prepared by the solid- state reaction method and the effects of substitution by Nb^{+5} in Y123 . However, the zero resistance transition temperature Structural and Electrical Properties of niobium doped $Y_{1-x}Nb_xBa_2Cu_3O_{7-0}$ Superconducting samples have been investigated. . It also showed that the normal resistivity of Nb doped YBCO compound samples were increased. Besides, desired value of Nb substituted YBCO sample with x=0.01, 0.02, 0.05 displays higher resistivity in normal state and higher J_c and pinning force, F_p values. So an enhancement can be beneficial in J_c of Nb substituted YBCO compounds for the practical applications of these high temperature superconducting materials.

References

1. J G Bednorz and K A Muller, *Zeitschrift für Physik B Condensed Matter* **64** (1986) 189.
2. M K Wu, J R Ashburn, C J Tong, P H Hor, R L Meng, L Gao, Z H Huang, Y O Wang, and C W Chu, *Physical Review Letters* **58** (1987) 908.
3. J W Ekin, A I Braginski, A J Panson, M A Janocko, D W Capone, N J Zaluzec, B Flandermeyer, O F de Lima, M Hong, J Kwo, and S H Liou, *Journal of Applied Physics* **62** (1987) 4821.
4. S Kim, S Zhou, Y Hu, M Acik, Y J C Berger, W De Here, A Bongiorno, and E Riedo, *Nat. Mater*. **11** (2012) 544.
5. X S Wu, S S Jiang, J Lin, J S Liu, and W M Chen, *X. Jin, Phys*. C **309** (1998) 25.
6. R Giri, V P S Awana, H K Singh, R S Tiwari, and O N Srivastava, *Anurag Gupta,B. V. Kumaraswamy, H. Kishan, Phys.* C **419** (2005) 101.
7. M Karppinen and H Yamauchi, *J Inorg. Mater*. **2** (2000) 589.
8. J J Capponi, C Chaillont, A W Hewat, P Lejay, M Mariezio, N Nguyou, B Raveau, J L Sonbeyroux, J Tho-lence, and R Tounier, *Eur. Phys. Lett*. **3** (1987) 1301.
9. H Yamauchi, M Karppinen, *Supercond. Sci. Technol*. **13** (2000) R 33.
10. R Beyers and T M Shaw, *Solid State Phys*. **42** (1989) 135.
11. N P Liyanawaduge, A Kumar, B S B Karunarathne, V P S Awana, *Journal of Superconductivity and Novel Magnetism* **25** (2012) 31.
12. N P Liyanawaduge, A Kumar, R Jha, B S B Karunarathne, and V P S Awana, *J. Alloys & Compd.* **74** (2012) 1.
13. C G S Pillai and A M George, "*Substitution of Copper by Niobium in Superconducting YBa2Cu3O7-δ*," *Journal of Material Science Lett.* **23** (1992) 1639.
14. E K Nazarova, K Nenkov, G Fuchs, and K-H Muller, *Effects of Calcium Substitution on the Superconducting Properties of R1−xCaxBa2Cu3Oz (R = Eu, Gd, Er; 0 ≤ x ≤ 0.3) Polycrystalline Samples. Physica* C. **436** (2006) 25.
15. W E Farneth, R K Bordia, E M McCarron III, M K Crawford, and R B Flippen, *Solid State Commun*. **66** (1988) 953.
16. R M Hazen, L W Finger, R J Angel, C T Perwitt, N L Ross, H K Mao, C G Hadidiacos, P H Hor, R L Meng, and C. W Chu, *Phys. Rev*. **335** (1987) 7238.

17. M B Turkoz, S Nezir, C Terzioglu, A Varilci, G Yildirim, *J Mater Sci. Mater Electron* **24** (2013) 896.
18. B D Cullity, *Element of X-Ray Diffraction. Addison-Wesley Reading, Boston* (1978).
19. S D Obertelli, J R Cooper, and J LTallon, *Phys. Rev*. B 46 (22) (1992) 14928.
20. B Abeles, H L Pinch, and J I Gittleman, *Phys. Rev. Lett*. **35** (1975) 247.
21. B Abeles, H L Pinch, and J I Gittleman, *Phys. Rev. Lett*. **35** (1975) 247.
22. A Ozlark, I Duzgun, and S Celebi, *J. Alleys and compd*. **495** (2010) 104.
23. C P Bean, *Phys Rev let* **8** (1962) 250.
24. WC Chan, C H Chiang, and Y J Hsu, *Cryogenics* **50** (2010) 292.
25. Z D Yakinci, D M Gokhfed, E Altin, F Kurt, S Altin, S Demirel. M A Aksan and M E Yakinciy, *J. Mater Sci*: **24** (2013) 4790.
26. A Schmehl, B Goetz, R R Schuls, C W Schneider, H Bielefeldt, H Hilgenkamp, and J Mannhart, *Euophys. Lett*. **47** (1999) 110.
27. G Hammerl, A Schmehl, R R Schuls, B Gaoetz, H Bielefeldt, C W Shneider, H Hilegen kamp, and J Mannhart, *Nature* **407** (2000) 162.
28. B A Malik, M A Malik, and K Asokan, *Chinese Journal of the physics* **55** (2017) 170.